Magnetic Phase Transition in Co/Cu/Ni/Cu(100) and Co/Fe/Ni/Cu(100)

C. Won,[1] Y. Z. Wu,[1] A. Scholl,[2] A. Doran,[2] N. Kurahashi,[1] H. W. Zhao,[1,3] and Z. Q. Qiu[1,4]

[1]*Department of Physics, University of California at Berkeley, Berkeley, California 94720, USA*
[2]*Advanced Light Source, Lawrence Berkeley National Laboratory, Berkeley, California 94720, USA*
[3]*International Center for Quantum Structures, CAS, Beijing 100080, China*
[4]*Materials Science Division, Lawrence Berkeley National Laboratory, Berkeley, California 94720, USA*

(Received 16 December 2002; revised manuscript received 10 July 2003; published 30 September 2003)

Magnetic phase transitions in coupled magnetic sandwiches of Cu/Co/Cu/Ni/Cu(100) and Cu/Co/Fe/Ni/Cu(100) are investigated by photoemission electron microscopy. Element-specific magnetic domains are taken at room temperature to reveal the critical thickness at which the magnetic phase transition occurs. The results show that a coupled magnetic sandwich undergoes three types of magnetic phase transitions depending on the two ferromagnetic films' thickness. A phase diagram is constructed and explained in the process of constructing Monte Carlo simulations, which corroborate the experimental results.

DOI: 10.1103/PhysRevLett.91.147202 PACS numbers: 75.70.Cn, 79.60.Jv

The magnetic phase transition of two-dimensional (2D) magnetic systems is one of the intensely studied topics in condensed matter physics [1–5]. Recently magnetic phase transition in coupled ferromagnetic multilayers has attracted great attention because of its fundamental importance. Theoretically, Wang and Mills explored the magnetic long-range order in a magnetically coupled superlattice using a mean field theory and found two separate magnetic phase transitions [6]. Experimental investigation of this subject has occurred only recently, after the development of element-specific measurements using x-ray magnetic circular dichroism (XMCD). The experimental results showed that a magnetically coupled sandwich undergoes two separate phase transitions with one film's Curie temperature (T_C) altered by the interlayer coupling [7–9]. However, those experimental results cannot be explained by a mean field theory that gives a T_C shift of only one-tenth the level observed in the experiment [10]. More fundamentally, it is unclear whether the experiments have explored all types of magnetic phase transitions in a coupled magnetic system. In this Letter, we report our investigation of magnetically coupled Cu/Co/Cu/Ni/Cu(100) and Cu/Co/Fe/Ni/Cu(100) systems using the photoemission electron microscopy (PEEM) technique. We construct a phase diagram in the Co-Ni thickness plane and find that the system exhibits three types of magnetic phase transitions. A Monte Carlo simulation is performed to understand the experimental observations.

The experiment is performed at the Beamline 7.3.1.1 of the Advanced Light Source. A Cu(100) substrate is cleaned in an UHV chamber by cycles of Ar-ion sputtering and annealing. The samples of Co/Cu/Ni and Co/Fe/Ni are grown epitaxially onto the Cu(100) at room temperature and characterized by low-energy electron diffraction and reflection high-energy electron diffraction. The Co and Ni films are fabricated into cross wedges to permit their thickness control. A 10 ML Cu protection layer is grown on top of the samples. The magnetic domain images are constructed by taking the ratio of L_3 and L_2 edges utilizing the effect of XMCD [9]. All domain images shown in this paper have the size of 40 μm $\times$ 40 μm.

Because the T_C of a magnetic thin film increases with its thickness [4], thickness-dependent measurements of magnetization at a fixed temperature reveal a critical thickness at which the magnetic phase transition occurs and a reduction of the critical thickness at a fixed temperature corresponds to an increase of the T_C at a fixed thickness [9]. In our experiment, we acquire element-specific magnetic domain images of the Ni and Co films as a function of film thickness at room temperature and obtain the critical thickness at which the magnetic domains appear. We find three types of magnetic phase transitions. Here we have chosen three samples to illustrate these transition types. The type-1 transition is represented in Fig. 1(a). For the Cu/Co(0.6 ML)/Cu(2 ML)/Ni(4.9–6.2 ML)/Cu(100) sample, the Ni film shows clear magnetic domains above 5.3 ML while the Co film shows no magnetic domains. This result shows that while the Co film is in the paramagnetic (PM) state, the Ni film undergoes a transition from PM below 5.3 ML to ferromagnetic (FM) above 5.3 ML. A similar result is observed in Cu/Co(2.0–2.4 ML)/Cu(2 ML)/Ni(1.7 ML)/Cu(100) where the Ni film is in the PM state and the Co film undergoes the PM-FM transition at $\sim$2.1 ML thickness. The type-2 transition is shown in Fig. 1(b). For the Cu/Co(2.7 ML)/Cu(2 ML)/Ni(2.5–5.3 ML)/Cu(100) sample, the Co film is in the FM state and the Ni film undergoes the PM-FM transition at $\sim$3.4 ML thickness. For the Cu/Co(0.7–1.2 ML)/Cu(2 ML)/Ni(6.0 ML)/Cu(100) sample, the Ni film is in the FM state and the Co film undergoes a phase transition at $\sim$0.9 ML thickness. The type-3 transition is presented in Fig. 1(c) which shows the magnetic domain images of Cu/Co(1.7 ML)/Cu(2 ML)/Ni(3.7–5.4 ML)/Cu(100) and

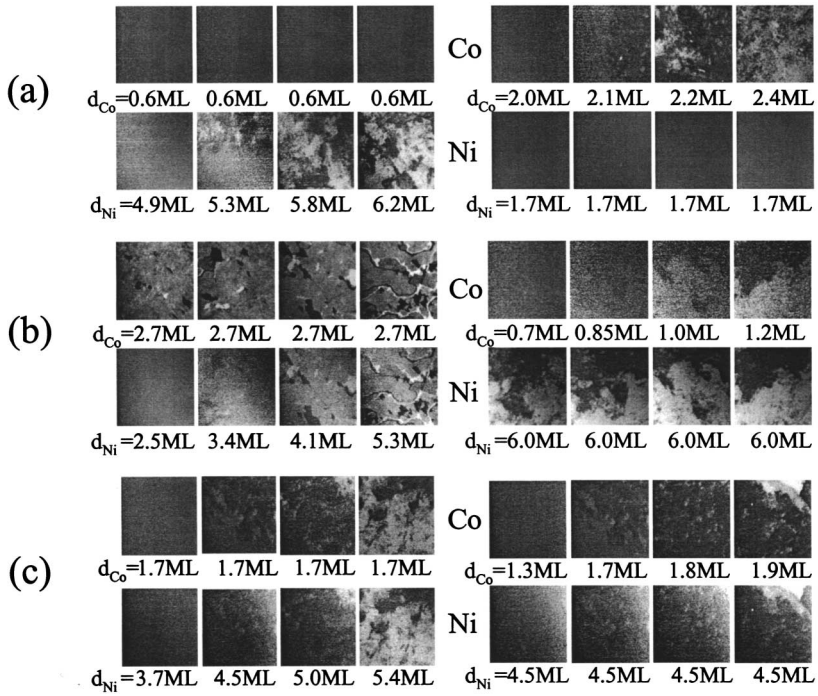

FIG. 1. Co and Ni magnetic domain images of Cu/Co/Cu(2 ML)/Ni/Cu(100). (a) Type-1 transition: one film is in the PM state and the other film undergoes the PM-FM transition; (b) type-2 transition: one film is in the FM state and the other film undergoes the PM-FM transition; and (c) type-3 transition: the Co and Ni films undergo the PM-FM transition simultaneously.

Cu/Co(1.3–1.9 ML)/Cu(2 ML)/Ni(4.5 ML)/Cu(100). In this type of transition, the Co and Ni magnetic domains appear simultaneously, indicating the existence of only a single PM-FM transition for both the Co and Ni films.

A magnetic phase diagram was then constructed in the Co-Ni thickness plane, plotting the critical thickness values of the Co and Ni layers [Fig. 2(a)]. The error bars in Fig. 2 represent the thickness uncertainties of the PM-FM transition. The Co and Ni layer's critical thicknesses divide the phase diagram into four regions (I–IV). Therefore the type-1 phase transition shown in Fig. 1(a) corresponds to the transition between I–II and I–III where one of the Co and Ni films is in the PM state and the other undergoes the PM-FM transition. The type-2 phase transition shown in Fig. 1(b) corresponds to the transition between II–IV and III–IV where one film is in the FM state and the other undergoes the PM-FM transition. The type-3 phase transition shown in Fig. 1(c) corresponds to the transition between I–IV where both

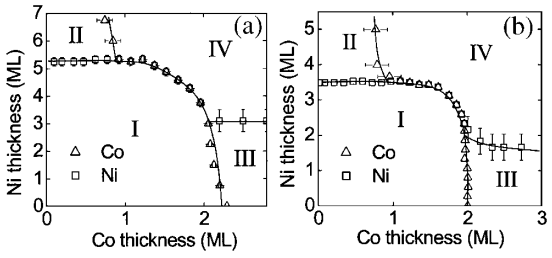

FIG. 2. Phase diagram of the magnetic phases of the (a) Cu/Co/Cu(2 ML)/Ni/Cu(100) and (b) Cu/Co/Fe(5 ML)/Ni/Cu(100). The triangles and squares are the Co and Ni films' critical thickness (respectively) at which the PM-FM transition occurs. The solid lines are simply to guide the eye.

films undergo the PM-FM transition simultaneously. A similar phase diagram is also obtained with the use of a fcc Fe spacer layer [Fig. 2(b)]. Thus the phase diagram shown in Fig. 2 should be a general result for a coupled magnetic sandwich.

From the phase diagram [Fig. 2(a)] we see that Co film in the range $0 < d_{Co} < 0.9$ ML stays in the PM states, and does not affect Ni's critical thickness (~ 5.3 ML) as compared with that of a Co-free Cu/Ni/Cu(100) system ($d_{Co} = 0$). With increasing Co thickness, the Ni critical thickness decreases from 5.3 ML and eventually approaches a constant value of $\sim$3.2 ML. This result shows that the Co layer in the FM state reduces the Ni critical thickness. The Co film behaves similarly—magnetic order of the Ni film reduces the critical thickness of the Co film. As either of the Ni and Co films approaches zero thickness, the other film exhibits a critical thickness: $d_{Co} \approx 2.2$ ML for Cu/Co/Cu(100) and $d_{Ni} \approx 5.3$ ML for Cu/Ni/Cu(100) at room temperature. These values agree reasonably well with the literature values [11–13].

To understand the experimental observations, we performed a Monte Carlo simulation of a magnetically coupled sandwich. Monte Carlo simulations have proven very successful for 2D magnetic systems [14,15]. To develop an appropriate simple model without losing important physics, we need to attend to the following two facts. First, the role of Co and Ni film thickness in our experiment is to change the T_C of the Co and Ni films. It has been shown that the T_C of an ultrathin ferromagnetic film is directly proportional to the number of pairwise spin-spin interactions in a spin cluster of the size of the interaction range; i.e., the role of the film thickness in the ultrathin regime is to rescale the exchange interaction by a factor directly proportional to the film thickness [4].

Therefore it is reasonable to map the Co (or Ni) film of a different thickness to a 2D ferromagnetic lattice of a different exchange interaction (J). This is the first simplification in our modeling. Second, for an XY model plus a fourfold magnetic anisotropy (corresponding to the Co and Ni films), it was shown that the effect of the anisotropy field is to develop a discrete phase where the system orders into one of the four preferred directions all the way up to the T_C [16]. Thus for the purpose of T_C study, we argue that the Co and Ni films can be appropriately represented by a planar four-state Potts model [17]. Further simplification is possible because it has been proven that a four-state Potts model is reducible to an Ising model [18]. With the above discussions, we modeled the Cu/Co/Cu/Ni/Cu(100) by two 2D Ising lattices plus an interlayer coupling. The Hamiltonian of the system is taken to be

$$H = -J_1 \sum_{\langle ij \rangle} S_{1i} S_{1j} - J_2 \sum_{\langle ij \rangle} S_{2i} S_{2j} - J_{\text{int}} \sum_{i} S_{1i} S_{2i}. \quad (1)$$

Here J_1 and J_2 are the magnetic exchange interactions of layer 1 and layer 2, and J_{int} is the interlayer coupling between layer 1 and layer 2. The summation in each layer is over the nearest neighbor pairs and each spin takes the value of ± 1. 200×200 lattice sites are employed in the simulation. Magnetic susceptibility is also derived from the simulation using $\chi = (1/k_B T)[\langle M^2 \rangle - \langle M \rangle^2]$, where M is the magnetization. It is well known that the divergence of susceptibility indicates the magnetic phase transition.

Figure 3 shows the simulation results for the magnetization (averaged spin) and the susceptibility of the two magnetic layers. The magnetization of the decoupled case ($J_{\text{int}} = 0$) is also shown for comparison. The Boltzmann constant is taken to be $k_B = 1$ for simplicity. Since there are only two independent variables in Eq. (1), we fix the value of $J_{\text{int}} = 1$ for the coupled sandwich and run the simulation for different values of J_1 and J_2. We find that in a certain range of J_1 and J_2, the two separate phase transitions of the decoupled layers merge into a single transition [Fig. 3(a)]. The magnetic susceptibility shows a singularlike peak at the transition, and the T_C of the coupled case is higher than those of the decoupled case. This is the type-3 transition observed in the experiment [Fig. 1(c)]. The merger of the two transitions into a single transition is due to the coupling of the magnetic fluctuations of the two layers. For other values of J_1 and J_2, the simulation result shows two separate transition temperatures [Fig. 3(b)] with the magnetic susceptibility showing a singularlike peak at the higher Curie temperature (T_C^{high}) and a small resonancelike peak at the lower Curie temperature (T_C^{low}). The transition at T_C^{high} corresponds to the type-1 transition [Fig. 1(a)] and the transition at T_C^{low} corresponds to the type-2 transition [Fig. 1(b)] in the experiments. For a given temperature, the PM-FM boundary can be obtained from the simulation for each of the two Ising lattices, thus we constructed the magnetic phase diagram in the J_1-J_2 plane at fixed

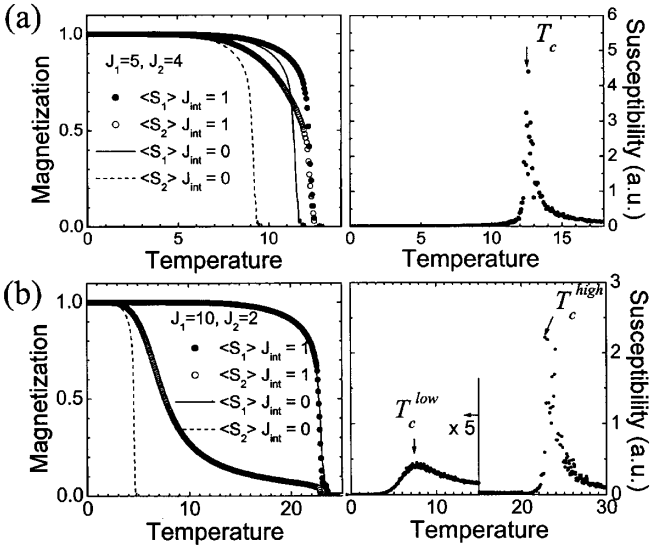

FIG. 3. Magnetization and susceptibility calculated by Monte Carlo simulation. (a) $J_1 = 5$, $J_2 = 4$; (b) $J_1 = 10$, $J_2 = 2$. Solid and dashed lines show calculations for the decoupled case.

temperature. The calculated phase diagram shows four regions (I–IV) in the J_1-J_2 plane, which correspond exactly to the four regions in the experiment (Fig. 2). Therefore the similarity of the calculated (Fig. 4) and experimental (Fig. 2) phase diagrams shows that the Monte Carlo simulations successfully reproduce the experimental observations. To make a numerical estimation, we take $J_{\text{int}} \approx 3$ meV as the interlayer coupling across 2 ML Cu [7]. Then $T = 5J_{\text{int}}$, $T = 10J_{\text{int}}$ in the simulation correspond to $T = 174$ K and $T = 348$ K. Thus Fig. 4(b) is close to the room temperature case. From Fig. 4(b) we see that the interlayer coupling reduces the J from $J_1/J_{\text{int}} = J_2/J_{\text{int}} \approx 4.2$ at the I/III and I/II boundaries to $J_1/J_{\text{int}} = J_2/J_{\text{int}} \approx 2.8$ at the II/IV and III/IV boundaries; i.e., the $J_{\text{int}} \approx 3$ meV decreases the J by $\Delta J = (4.2\text{–}2.8)J_{\text{int}} \approx 4.2$ meV. Assuming a linear thickness dependence of

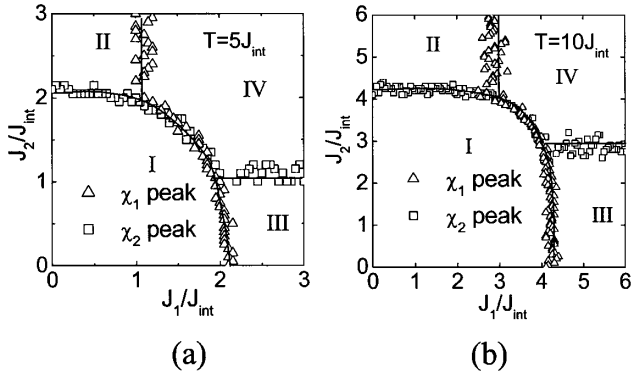

FIG. 4. Phase diagram of the Monte Carlo simulations in the J_1-J_2 plane. Four regions are identified, which correspond to the four regions in Fig. 2. Temperatures used in the calculations are (a) $T = 5J_{\text{int}}$ and (b) $T = 10J_{\text{int}}$. The solid lines are to guide the eye.

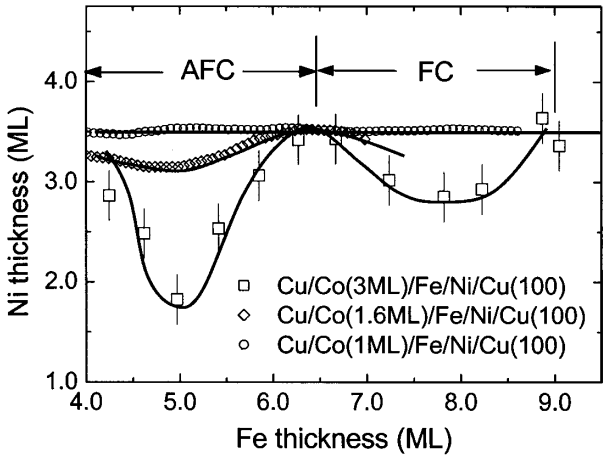

FIG. 5. Ni critical thickness versus the Fe spacer layer thickness of Cu/Co/Fe/Ni/Cu(100). The 1, 1.6, and 3 ML Co samples represent the Ni critical thickness at the I/II, I/IV, and III/IV boundaries of the phase diagram. The solid lines are to guide the eye.

the T_C [4] and noticing that the T_C of a 2D Ising lattice is $T_C = 2J/k_B \ln(1 + \sqrt{2})$, the reduction of $\Delta J \approx 4.2$ meV due to the interlayer coupling in Fig. 4(b) should result in a reduction of the critical thickness of $\Delta d = [2d_0 \Delta J/k_B T_C(d_0) \ln(1 + \sqrt{2})]$, where $T_C(d_0)$ is the Curie temperature of a single film with d_0 thickness. Taking $T_C(2.2\ \text{ML}) = 300$ K for Co and $T_C(5.3\ \text{ML}) = 300$ K for Ni, the reduction of the critical thickness for Co and Ni films is estimated to be $\Delta d_{\text{Co}} \approx 0.8$ ML and $\Delta d_{\text{Ni}} \approx 2.0$ ML, which agree reasonably well with the experimental results [Fig. 2(a)].

We further studied the Ni critical thickness as a function of the fcc Fe spacer layer thickness in Cu/Co/Fe/Ni/Cu(100). We first confirmed the Ni-Co oscillatory interlayer coupling by analyzing the Ni and Co domain colors and found that Ni and Co layers process antiferromagnetic coupling (AFC) for $4.5\ \text{ML} < d_{\text{Fe}} < 6.5\ \text{ML}$ and ferromagnetic coupling (FC) for $6.5\ \text{ML} < d_{\text{Fe}} < 9\ \text{ML}$, in agreement with our previous result [9]. We then studied the Ni critical thickness of Cu/Co/Fe(wedge)/Ni(wedge)/Cu(100) at $d_{\text{Co}} \approx 1$, 1.6, and 3 ML (Fig. 5). The reason for choosing 1, 1.6, and 3 ML Co is to have the Ni phase transition occur at the I/II, I/IV, and III/IV boundaries, respectively. We find that the Ni critical thickness at the I/II boundary does not depend on the interlayer coupling. This result agrees with the simulation result that the PM Co has little effect on the Ni phase transition. However, the Ni critical thickness at the I/IV boundary and the III/IV boundary oscillates with the Fe film thickness, with the critical thickness reduced in both the AFC and FC regions. Furthermore, the oscillation amplitude at the I/IV boundary is smaller than that at the III/IV boundary and the Ni critical thickness reaches its maximum value at the zero interlayer coupling. These observations further confirm that the reduction of the Ni critical thickness at the I/IV and III/IV boundaries in Fig. 2, as compared with the Ni critical thickness at the I/II boundary, comes from the Ni-Co interlayer coupling. The similarity between the effects of the AFC and FC on the reduction of the critical thickness can be easily understood from Eq. (1) because the Hamiltonian is invariant under the action of $J_{\text{int}} \rightarrow -J_{\text{int}}$ and $\overline{S} \rightarrow -\overline{S}_1$ (or $\overline{S}_2 \rightarrow -\overline{S}_2$).

In summary, the magnetic phase transitions in Cu/Co/Cu/Ni/Cu(100) and Cu/Co/Fe/Ni/Cu(100) were investigated by PEEM. We found that a coupled magnetic sandwich exhibits three types of magnetic phase transitions. A magnetic phase diagram was constructed in the Co-Ni thickness plane. Monte Carlo simulations on two coupled 2D Ising lattices successfully reproduce the experimental observations.

This work was supported by the National Science Foundation under Contract No. DMR-0110034, the U.S. Department of Energy under Contract No. DE-AC03-76SF0098, and the ICQS of the Chinese Academy of Sciences.

[1] V. L. Pokrovsky, J. Magn. Magn. Mater. **200**, 515 (1999).
[2] N. D. Mermin and H. Wagner, Phys. Rev. Lett. **17**, 1133 (1966).
[3] M. Bander and D. L. Mills, Phys. Rev. B **38**, 12 015 (1988).
[4] Renjun Zhang and Roy F. Willis, Phys. Rev. Lett. **86**, 2665 (2001).
[5] Z. Q. Qiu, J. Pearson, and S. D. Bader, Phys. Rev. Lett. **67**, 1646 (1991).
[6] R. W. Wang and D. L. Mills, Phys. Rev. B **46**, 11 681 (1992).
[7] U. Bovensiepen, F. Wilhelm, P. Srivastava, P. Poulopoulos, M. Farle, A. Ney, and K. Baberschke, Phys. Rev. Lett. **81**, 2368 (1998).
[8] A. Ney, F. Wilhelm, M. Farle, P. Poulopoulos, P. Srivastava, and K. Baberschke, Phys. Rev. B **59**, 3938 (1999).
[9] Y. Z. Wu, C. Won, A. Scholl, A. Doran, F. Toyoma, X. F. Jin, N. V. Smith, and Z. Q. Qiu, Phys. Rev. B **65**, 214417 (2002).
[10] P. J. Jensen, K. H. Bennemann, P. Poulopoulos, M. Farle, F. Wilhelm, and K. Baberschke, Phys. Rev. B **60**, 14 994 (1999).
[11] C. M. Schneider, P. Bressler, P. Schuster, J. Kirschner, J. J. de Miguel, and R. Miranda, Phys. Rev. Lett. **64**, 1059 (1990).
[12] L. H. Tjeng, Y. U. Idzerda, P. Rudolf, F. Sette, and C. T. Chen, J. Magn. Magn. Mater. **109**, 288 (1992).
[13] M. Tischer, D. Arvanitis, T. Yokoyama, T. Lederer, L. Troger, and K. Baberschke, Surf. Sci. **307–309**, 1096 (1994).
[14] I. Booth, A. B. MacIsaac, J. P. Whitehead, and K. De'Bell, Phys. Rev. Lett. **75**, 950 (1995).
[15] Carsten Timm, S. M. Girvin, Patrik Henelius, and Anders W. Sandvik, Phys. Rev. B **58**, 1464 (1998).
[16] Jorge V. José, Leo P. Kadanoff, Scott Kirkpatrick, and David R. Nelson, Phys. Rev. B **16**, 1217 (1977).
[17] F. Y. Wu, Rev. Mod. Phys. **54**, 235 (1982).
[18] D. D. Betts, Can. J. Phys. **42**, 1564 (1964).